Applications of Shape-Optimised Cold-Formed Steel Cross-Sections in Roof Purlin and Wall Stud Construction

Ziqi ZHAO*, Zichen WEI[a], Hong GUAN[a], Bin WANG[b], Huiyue QIAO[a]

*School of Engineering and Built Environment, Griffith University, QLD 4222, Australia

ziqi.zhao@griffithuni.edu.au

[b] Xstructe Consulting, QLD 4109, Australia

Abstract

Cold-formed steel (CFS) members are widely used in low-to-medium rise light steel building construction due to their lightweight, fabrication versatility and low production costs. Optimising the conventional CFS (CCFS) members for enhanced load-bearing capacity and less material consumption will lead to efficient and economical construction solutions. This study presents two applications of (i) an optimised folded-flange lipped channel sections for roof purlins and (ii) an optimised folded-flange "*Sigma*" sections for wall studs. The aim of this study is to minimise the cross-sectional areas of the individual shape-optimised CFS sections with the same load-bearing capacity as the corresponding CCFS ones for these applications. The optimisation process for each application results in five shape-optimised sections having 100%, 80%, 60%, 40% and 20% of the cross-sectional area of the CCFS section. The elastic buckling analyses of all the optimised CFS sections are conducted using *CUFSM* software based on the Finite Strip Method (FSM), and the obtained buckling stresses are used to determine the nominal capacity of each optimised CFS sections using the Direct Strength Method (DSM). The area-capacity curves for the five shape-optimised sections indicate that the cross-sectional areas of the optimal CFS cross-sections for a roof purlin and a wall stud are 89.2% and 52.7% of the CCFS area, respectively. Furthermore, a finite element analysis of the obtained optimal cross-sections is conducted in *Strand7* to validate the reliability of the optimisation process.

Keywords: Cold-formed steel (CFS), shape-optimised sections, optimal cross-sectional area, load-bearing capacity, finite element analysis

1. Introduction

Cold-formed steel (CFS) is a kind of semi-finished or finished product made from rolled or pressed thin-walled coiled or flat bars without any heat treatment. Due to the high strength-to-weight ratio, dimensional stability, flexibility in cross-sectional profiles, and ease of fabrication and transportation, CFS is considered a more cost-effective construction material being widely used in low-to-medium rise light steel buildings and modular construction [1,2]. Conventional cold-formed steel (CCFS) members are mainly available in *Cee*, *Zed* and *Sigma* profiles with or without local stiffeners (Figure 1). They are commonly used as flexural members of structural frames for specific applications such as roof purlins, girts and wall studs [3] (Figure 2(a)). Due to its thin-walled nature, the strength and efficiency of a CFS cross-section are usually governed by a combination of three basic modes of buckling, viz. local, distortional and global buckling, which are closely related to the shape of the CFS section [4]. The Direct Strength Method (DSM) [5], by integrating the computational stability analysis into the design process, can be used to determine the capacity of members accounting for these three buckling modes. DSM is based on the elastic buckling analysis and has the advantage of dealing with the entire section of the CFS member rather than on individual elements [6].

Optimisation of CCFS members can increase load-bearing capacity and reduce material consumption. Such an enhancement at the component level can also increase the overall capacity of the CFS frame system [7]. In general, the optimisation of CFS members can be divided into two categories: (i) shape optimisation, where the profile of the cross-section is changed to obtain an innovative shape [4,8,9], or (ii) size optimisation, where the optimal dimensions of the cross-section with a predefined shape can be obtained [10,11]. The study presented in this paper is focused on the size optimisation process for two shape-optimised sections (SOCFS) applied to roof purlins and wall studs, with the aim of minimising the cross-sectional areas of the individual SOCFS section with the same load-carrying capacity as the corresponding CCFS ones for these applications. The elastic buckling analyses of all the optimised CFS sections are conducted using *CUFSM* software based on the Finite Strip Method (FSM) [12], and the obtained buckling stresses are used to determine the nominal capacity of each optimised CFS member by DSM. Furthermore, a finite element analysis of the obtained optimal members is also conducted to validate the reliability of the optimisation process.
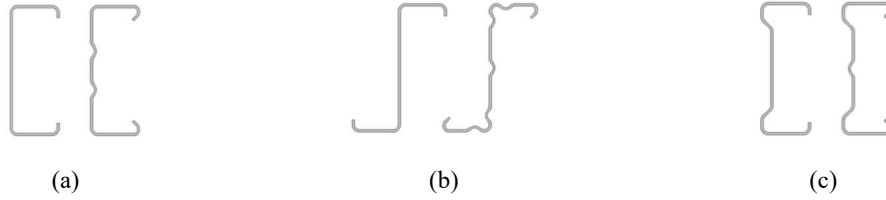

(a) (b) (c)

Figure 1. Conventional CFS sections with or without stiffeners, (a) "*Cee*", (b) "*Zed*", and (c) "*Sigma*".

2. Structural models

Two structural models are considered to investigate the optimisation problem: (i) a 2,100*mm* span, simply supported roof purlin subjected to a nominal bending moment M_b, with a shape-optimised folded-flange lipped channel section (Figure 2(b)), and (ii) a 2,400*mm* length, simply supported wall stud subject to an axial compressive load N_c, with a shape-optimised folded-flange "*Sigma*" section (Figure 2(c)).

The reference SOCFS cross-sections (Figures 3(b) and 4(b)), produced by Wang et.al [1], were optimised from the unconstrained simply-supported CFS beams. The previously developed augmented Lagrangian Genetic Algorithm (GA) [12] was used as the "self-shape" optimisation algorithm to find the new cross-section, which consists of minimising the cross-sectional area subject to an inequality penalty function (Eq. (1)) on a uniform bending moment M^* and a compressive axial load N^*.

$$\frac{N^*}{\phi_c N_c} + \frac{M^*}{\phi_b M_b} \leq 1 \tag{1}$$

where φ_c and φ_b are capacity reduction factors, taken as 1.0.

In this algorithm, GA is performed as the search algorithm by using the cross-over operator and mutation operator to generate superior offsprings, the Augmented Lagrangian (AL) method is combined as a powerful tool to avoid the ill-conditioned process by controlling the penalty factors remain finite [13]. The fitness function suitable for GA and AL was determined as Eq. (2) and Eq. (3), respectively.

$$f(GA) = \frac{A_s}{A_{ref}} + \alpha\{\max[0, (\frac{N^*}{\phi_c N_c} + \frac{M^*}{\phi_b M_b} - 1)]\} \tag{2}$$

where A_s is the cross-sectional area of the optimised cross-section, to remain finite, and A_{ref} is the reference area of similar value to the optimised cross-sectional area.

$$f(AL) = \frac{A_s}{A_{ref}} + \frac{1}{2}\{\gamma + [\max(0,(\frac{N^*}{\phi_c N_c} + \frac{M^*}{\phi_b M_b} - 1) + \mu)]^2\} \tag{3}$$

where γ is the penalty function coefficient, and μ is the real parameter to the penalty function.

The optimised folded-flange lipped channel section was obtained from the CCFS *Cee* section without stiffeners (Figure 3(a)), which can be characterised as a four-element (① to ④) per half cross-section type, in Figure 3(b), for the roof purlin model. The optimised folded-flange "*Sigma*" section was obtained from the CCFS *Cee* section with stiffeners (Figure 4(a)), in which the eight elements (① to ⑧) per half cross-section is the fittest to the wall stud model (Figure 4(b)).

The CCFS *Cee* cross-sections with and without stiffeners considered in this study were chosen from the design manuals *Rondo* [14]and *LYSAGHT* [15], respectively. The area of a cross section can be simply determined by multiplying its thickness by its perimeter. Note that the area and the thickness of the initial SOCFS (e.g. Figure 3(b)) are the same as those of the CCFS (e.g. Figure 3(a)). Note also that the aspect ratio remains the same for CCFS and SOCFS. Thereafter, the total length of all the elements in an individual SOCFS can be derived. Then the length of each element that forms the cross-section can be mathematically calculated based on the element's orientation [1]. Since the aspect ratio and the thickness of the cross-section remain constant, reducing the length of each element in the initial SOCFS (e.g. Figure 3(b)) with the same proportion can result in a correspondingly reduced cross-sectional area of the subsequent SOCFS (e.g. Figures 3(c) to (f)). In this study, the cross-sectional area of the SOCFS is gradually reduced to 80%, 60%, 40% and 20% of the CCFS section (A_{CS}), for both roof purlin and wall stud members.
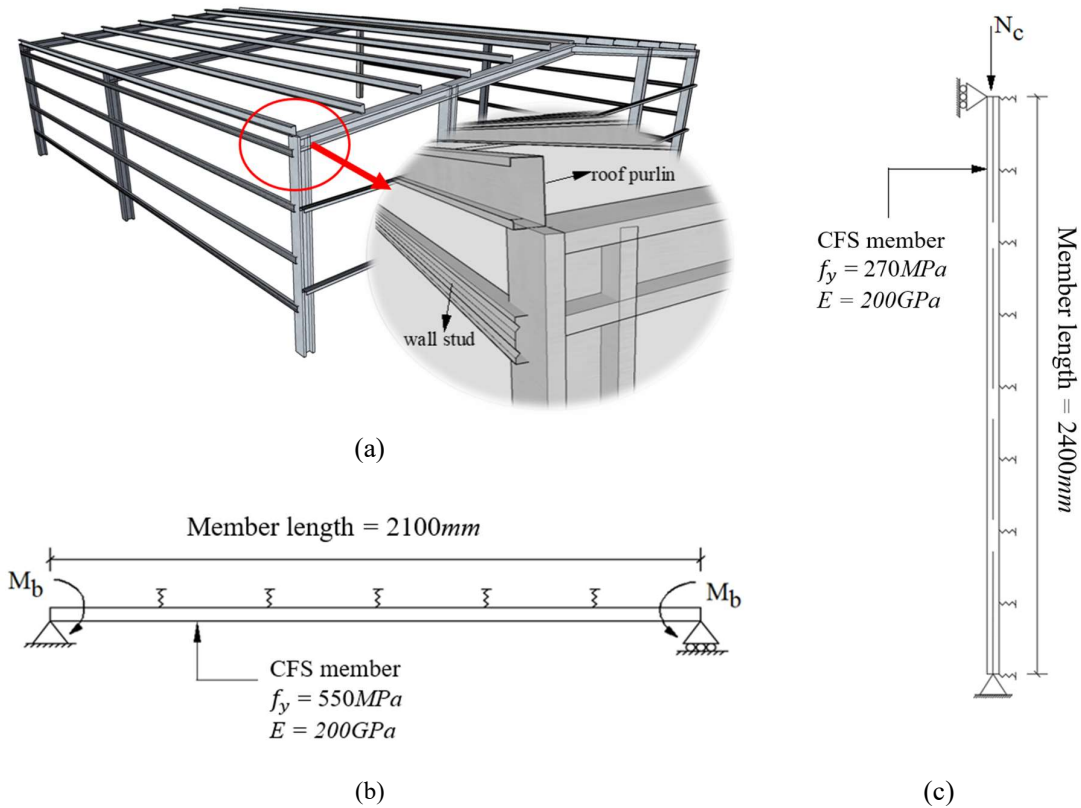

(a)

(b)

(c)

Figure 2. Structural models for the optimisation problem: (a) structural frames, (b) roof purlin and (c) wall stud.
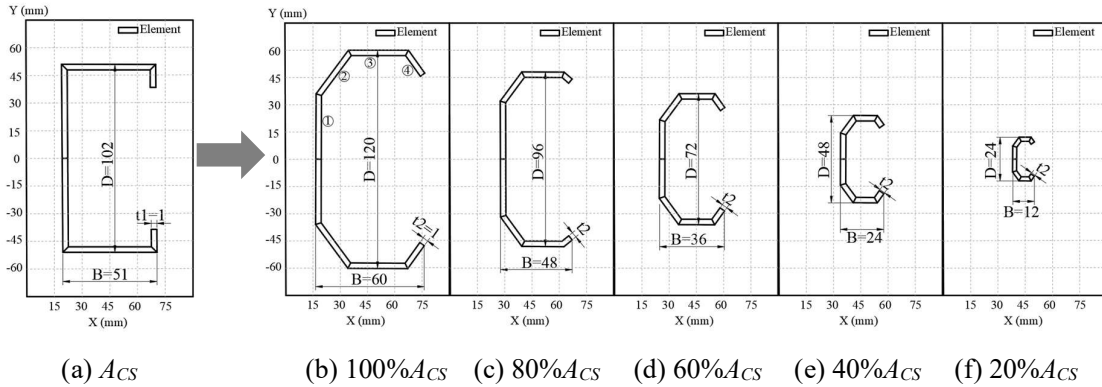
(a) A_{CS} (b) $100\%A_{CS}$ (c) $80\%A_{CS}$ (d) $60\%A_{CS}$ (e) $40\%A_{CS}$ (f) $20\%A_{CS}$

Figure 3. Dimensions of CCFS and shape-optimised cross-sections for roof purlin cross-section.

(a) A_{CS} (b) $100\%A_{CS}$ (c) $80\%A_{CS}$ (d) $60\%A_{CS}$ (e) $40\%A_{CS}$ (f) $20\%A_{CS}$
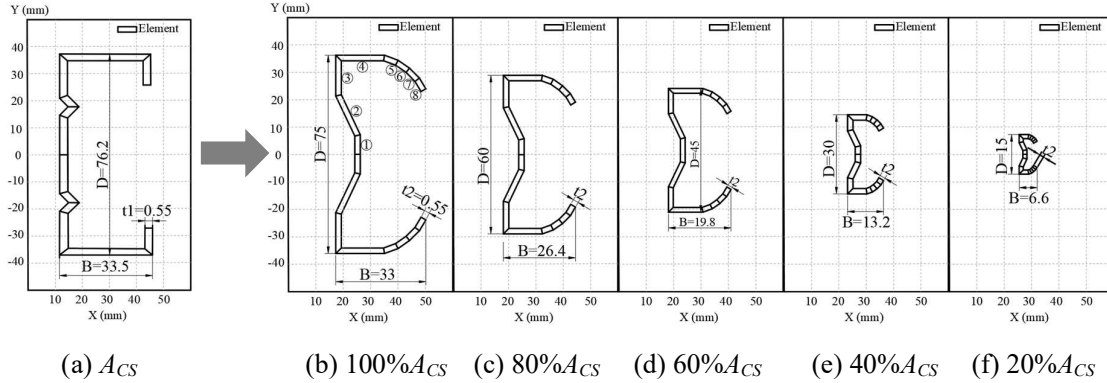
Figure 4. Dimensions of CCFS and shape-optimised cross-sections for wall stud cross-section.

3. Numerical analysis

3.1. Elastic buckling analysis

Elastic buckling analysis is a technique for determining the buckling loads and deformed shapes when a structure becomes buckled and unstable. It allows to obtain the buckling stress f_o under the corresponding buckling modes, which can subsequently be used to determine the bearing capacity of the CFS cross-sections. In this study, the elastic buckling analyses were carried out using the software *CUFSM*, which was developed based on the Finite Strip Method (FSM) and can provide a quick analysis to obtain the buckling load factors by entering the basic parameters, such as the element coordinates, dimension and thickness, and the expected loads of the CFS sections. The obtained buckling load factors are expressed as the ratio of the elastic buckling stress f_o to the steel yield stress f_y. The principles for distinguishing and determining the three buckling load factors, viz. f_{oe}/f_y (global buckling), f_{ol}/f_y (local buckling) and f_{od}/f_y (distortional buckling), are described in detail in Section 4.2. Table 1 and Table 2 list the obtained local (f_{ol}/f_y) and distortional (f_{od}/f_y) load factors for each cross-section of the roof purlin and wall stud members. The buckling stresses f_{ol} and f_{od} can then be determined which are also given in Tables 1 and 2.

3.2. Bearing behaviour

The Direct Strength Method (DSM) was used in this study to calculate the bearing capacity of all cross-sections. It is based on AS/NZS 4600 [16] and employs the strength curves on the entire CFS member rather than the isolated cross-sectional elements [17]. The DSM allows the calculation of the nominal bearing capacities under local, distortional and global buckling modes by using the corresponding buckling stresses and the design bearing capacity is determined as the minimum of these three values. In this study, the design bending moment applied to the roof purlin structural model can be determined as

$$M_b = \min (M_{bl}, M_{bd}, M_{be}) \tag{4}$$

where M_{bl}, M_{bd}, and M_{be} are the nominal bending capacities for local, distortional, and global buckling modes, respectively.

Similarly, the design axial compressive load applied to the wall stud structural model was expressed as

$$N_c = \min (N_{cl}, N_{cd}, N_{ce}) \tag{5}$$

where N_{cl}, N_{cd}, and N_{ce} are the nominal axial compressive capacities for local, distortional, and global buckling modes, respectively.

The calculated M_b and N_c for the roof purlin and wall stud cross-sections are also summarised in Table 1 and Table 2, respectively.

4. Results and discussion

4.1. Optimal cross-sectional area

According to Table 1 and Table 2, the piecewise linear area-capacity curves for the five SOCFSs can be plotted for the roof purlin and the wall stud structural models, respectively, in Figures 5(a) and (b). It can be seen that the initial SOCFS with a cross-sectional area of $100\%A_{CS}$ (e.g. point B1 in Figure 5(a)) has a greater bearing capacity than the CCFS (e.g. point A1 in Figure 5(a)) for both roof purlin and wall stud sections, which validates the shape optimisation outcomes that the SOCSF has a higher strength than that of the corresponding CCFS with the same cross-sectional size [1]. By drawing a horizontal line from the CCFS point (e.g. point A1), an intersection point with the plotted area-capacity curve, denoted as a blue triangle in the diagram, was obtained indicating that the optimal SOCFS has the same load carrying capacity as the CCFS. Given the linear relation between every two adjacent SOCFS points on the area-capacity curve, the cross-sectional areas of the optimal SOCFSs for the roof purlin and wall stud sections can be determined by linear interpolation.

Specifically, for the roof purlin member, the optimal SOCFS point in Figure 5(a) falls between points B1 and C1, on a linear line which can be expressed as

$$y = 0.0214x - 1.65 \tag{6}$$

where x is the cross-sectional area and y is the bending moment capacity.

By substituting the same bending moment capacity of 2.72 *kNm* as the CCFS into Eq. (6), the optimal cross-sectional area of the roof purlin member is determined to be 204.2mm^2, which is only $89.2\%A_{CS}$.

Similarly, the optimal SOCFS point for the wall stud member falls between points D2 and E2 in Figure 5(b), also on a linear line which can be expressed as

$$y = 0.1646x + 3.1872 \tag{7}$$

where x is the cross-sectional area and y is the axial compressive capacity.

Taking the same axial compressive capacities of the SOCFS and CCFS of $10.73kN$, the optimal cross-sectional area of the wall stud member can be calculated using Eq. (7) as $45.85mm^2$, which is only $52.7\%A_{CS}$.

Table 1. Results of elastic buckling analysis and DSM for roof purlin cross-sections.

Cross-section naming	Cross-section area (mm^2)	Load factors		Steel yield stress	Buckling stress		Design bending moment M_b (kNm)
		f_{ol}/f_y	f_{od}/f_y	f_y (MPa)	f_{ol} (MPa)	f_{od} (MPa)	
A1 (A_{CS})	229	0.60	0.56	550	330.0	308.0	2.72
B1 (100%A_{CS})	229	1.21	0.77	550	665.5	423.5	3.25
C1 (80%A_{CS})	183.2	1.89	0.98	550	1039.5	539.0	2.27
D1 (60%A_{CS})	137.4	3.37	1.37	550	1853.3	753.3	1.43
E1 (40%A_{CS})	91.6	7.32	-	550	4026.0	-	0.7
F1 (20%A_{CS})	45.8	-	4.84	550	-	2662.0	0.14

Table 2. Results of elastic buckling analysis and DSM for wall stud cross-sections

Cross-section naming	Cross-section area (mm^2)	Load factors		Steel yield stress	Buckling stress		Design axial compressive load N_c (kN)
		f_{ol}/f_y	f_{od}/f_y	f_y (MPa)	f_{ol} (MPa)	f_{od} (MPa)	
A2 (A_{CS})	86.99	0.91	0.34	270	244.54	92.61	10.73
B2 (100%A_{CS})	86.99	2.96	0.80	270	799.47	216.27	16.06
C2 (80%A_{CS})	69.52	4.56	1.00	270	1231.2	270.0	14.08
D2 (60%A_{CS})	52.15	7.86	3.08	270	2122.2	831.6	11.77
E2 (40%A_{CS})	34.76	-	1.78	270	-	480.6	8.91
F2 (20%A_{CS})	17.39	-	4.88	270	-	1317.6	4.69
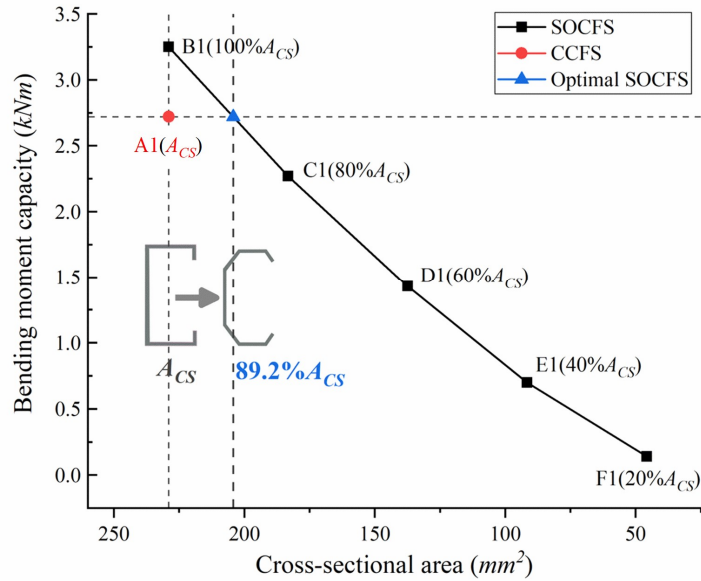
(a)
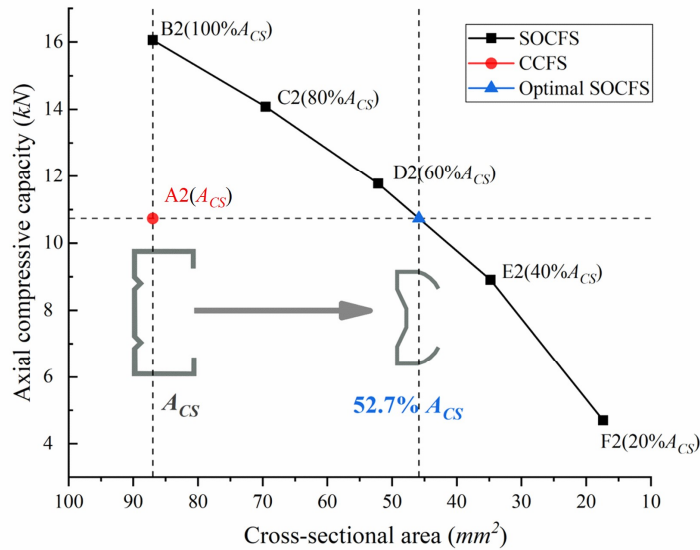
(b)

Figure 5. Area-capacity curves for (a) roof purlin and (b) wall stud.

4.2. Validation of CUFSM results using finite element analysis

In order to verify the accuracy of the optimal SOCFSs for the roof purlin and wall stud members as described above, a finite strip analysis in *CUFSM* and a finite element analysis in *Strand7* were performed. Note that the elastic local and distortional buckling modes cannot be distinctly identified in *Strand7*. Therefore, this validation study only focused on the global buckling mode which is readily obtainable in *Strand7* and *CUFSM*.

For the individual optimal roof purlin and wall stud sections, the buckling load factor (f_o/f_y) versus the half-wavelength (1/2 sine wave) from *CUFSM* is shown in Figure 6 in the form of the "signature curve". Ideally, each signature curve contains two local minima, the first one of which is usually considered to be the local buckling load factor (f_{ol}/f_y), and the second is the distortional buckling load factor (f_{od}/f_y) [12]. In the case where only one local minimum exists on this curve (Figure 6(b)), Gilbert et al. [4] suggested that if the buckling occurs at a half-wavelength being less than the perimeter length of the cross-section, this single minimum is regarded as the local buckling load factor; otherwise, it is deemed as distortional. Due to the simply-supported boundary condition, the global buckling generally exists at the end of the member, as shown in the elastic buckling analysis. Thus, the global buckling load factor (f_{oe}/f_y) is usually obtained when the half-wavelength equals the member length. Based on the above descriptions, the local, distortional, and global buckling modes for the optimal roof purlin cross-section can be clearly identified in Figure 6(a). However, no local buckling was identified on the signature curve for the optimal wall stud cross-section (Figure 6(b)), but only distortional and global buckling modes were distinguished.

The global buckling analysis in *Strand7* for the optimal roof purlin section resulted in a load factor equalling 0.48*MPa*, which is slightly higher that the corresponding *CUFSM* value of 0.35*MPa* (Figure 6(a)). Similarly, the load factor for the optimal wall stud section is 0.082*MPa* from *Strand7,* also slightly higher than the *CUFSM* value of 0.069*MPa* (Figure 6(b)). The disparity in the predicted load factors from the two analysis methods is due to the different ways they simulate the members, i.e., finite element versus finite strip. Nevertheless, such a discrepancy can be considered acceptable.

Figure 7 and Figure 8 show the *Strand7* initial shape and the corresponding deformed shape under the global buckling mode for the optimal roof purlin and wall stud structural models, respectively. The global buckling deformation of the roof purlin model is an apparent tilt of the whole CFS section (Figure 7(b)), while the deformation of the wall stud model is primarily a lateral movement of the web along the *x*-axis (Figure 8(b)). Compared to the global buckled shapes obtained from *CUFSM* as shown in Figure 6, the deformed shapes from *Strand7* are rather consistent. Therefore, the buckling analysis results of the optimal cross-sections obtained from *CUFSM* are well validated by *Strand 7*.
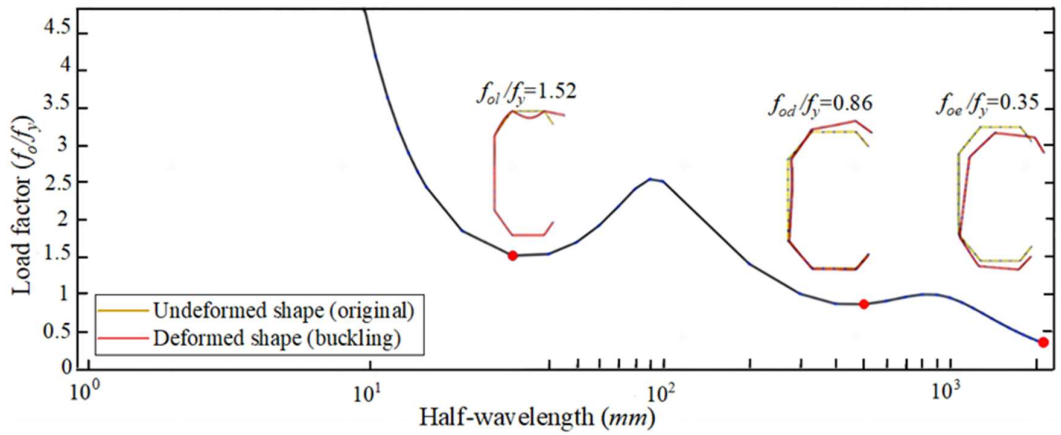
(a)
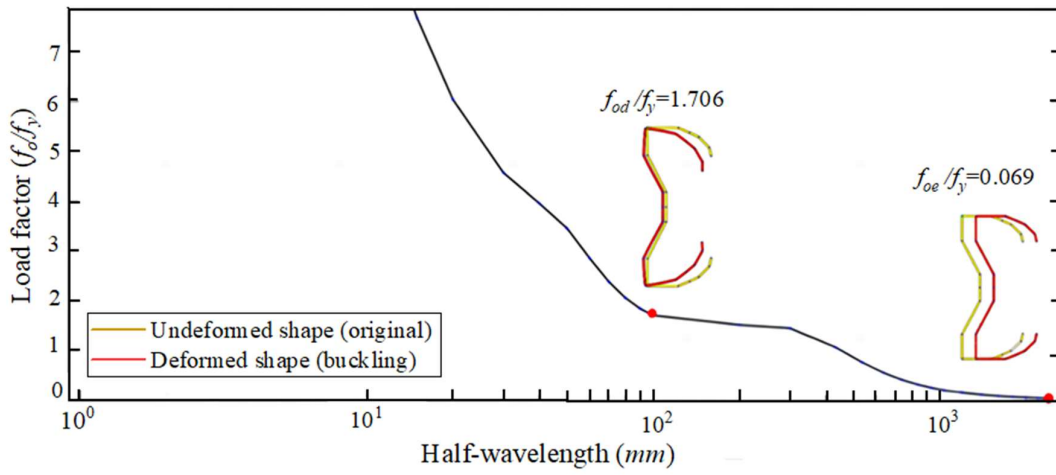
(b)

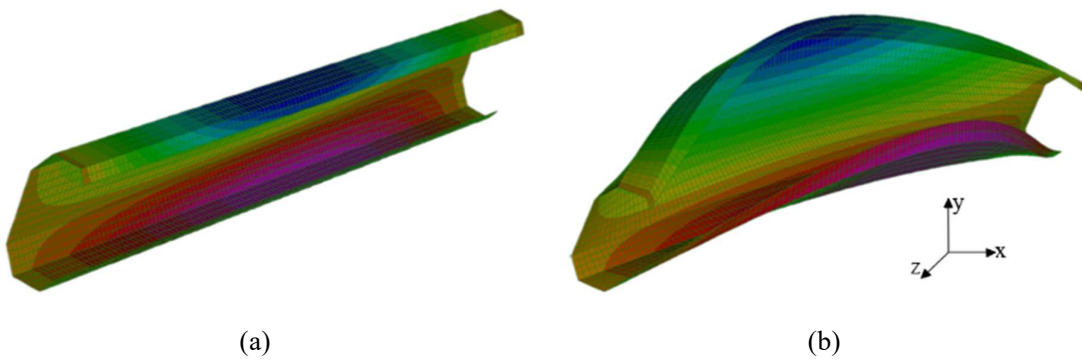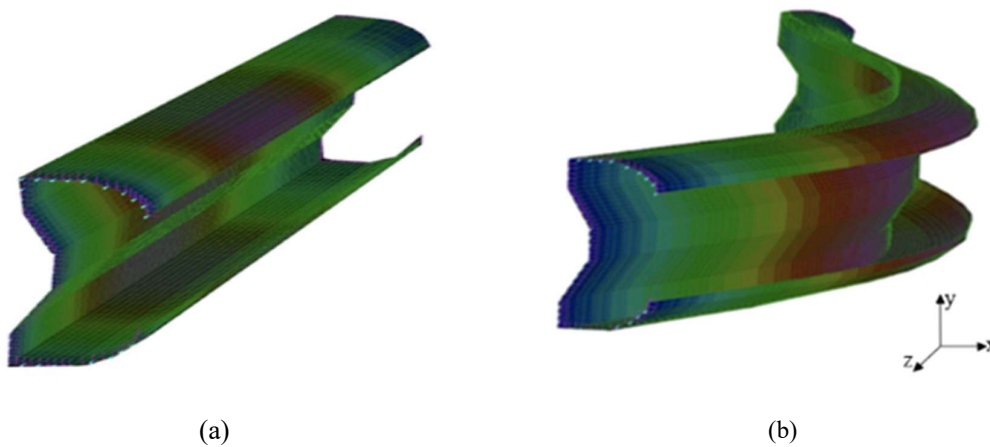Figure 6. Elastic buckling analysis of optimal SOCFSs for (a) roof purlin and (b) wall stud.

(a)   (b)

Figure 7. Deformed shape of the optimal roof purlin structural model in *Strand7*, (a) initial 3D model, and (b) global buckling mode.

(a)   (b)

Figure 8. Deformed shape of the optimal wall stud structural model in *Strand7*, (a) initial 3D model, and (b) global buckling mode.

5. Conclusion

This paper presents the size optimisation process of the individual shape-optimised cold-formed steel sections (SOCFSs) for roof purlin and wall stud structural models. For each model, a series of elastic buckling analyses and bearing capacity calculations were carried out using *CUFSM* and DSM, leading to an optimal SOCFS with a reduced cross-sectional area whilst maintaining the same load bearing capacity as the equivalent conventional CFS (CCFS). The cross-sectional areas of the optimal roof purlin and wall stud members are found to be 89.2% and 52.7% of that of the corresponding CCFS, respectively. Finite element analyses were also performed in *Strand7* on the two structural models with the optimal cross-sections, which verified the accuracy of the entire size optimisation process for SOCFSs using the finite strip method in *CUFSM*.

References

[1] B. Wang, B. P. Gilbert, A. M. Molinier, H. Guan, and L. H. Teh, "Shape optimisation of cold-formed steel columns with manufacturing constraints using the Hough transform," *Thin-Walled Structures*, vol. 106, pp. 75-92, 2016.

[2] B. W. Schafer, "Cold-formed steel structures around the world," *Steel Construction,* vol. 4, no. 3, pp. 141-149, 2011

[3] P. Gatheeshgar, K. Poologanathan, S. Gunalan, B. Nagaratnam, K. D. Tsavdaridis, and J. Ye, "Structural behaviour of optimized cold-formed steel beams," *Steel Construction*, vol. 13, no. 4, pp. 294-304, 2020.

[4] B. P. Gilbert, T. J.-M. Savoyat, and L. H. Teh, "Self-shape optimisation application: Optimisation of cold-formed steel columns," *Thin-walled structures*, vol. 60, pp. 173-184, 2012.

[5] *Direct Strength Method Design Guide*, American Iron and Steel Institute, 2006

[6] B. W. Schafer, "The direct strength method of cold-formed steel member design," *Journal of constructional steel research*, vol. 64, no. 7-8, pp. 766-778, 2008.

[7] D. T. Phan, S. M. Mojtabaei, I. Hajirasouliha, J. Ye, and J. B. Lim, "Coupled element and structural level optimisation framework for cold-formed steel frames," *Journal of Constructional Steel Research*, vol. 168, p. 105867, 2020.

[8] M. Moharrami, A. Louhghalam, and M. Tootkaboni, "Optimal folding of cold formed steel cross sections under compression," *Thin-Walled Structures*, vol. 76, pp. 145-156, 2014.

[9] V. M. Guimaraes, B. P. Gilbert, N. Talebian, and B. Wang, "Shape optimisation of singly-symmetric cold-formed steel purlins," *Thin-Walled Structures*, vol. 161, 2021.

[10] J. Lee, S.-M. Kim, and H. S. Park, "Optimum design of cold-formed steel columns by using micro genetic algorithms," *Thin-Walled Structures*, vol. 44, no. 9, pp. 952-960, 2006.

[11] B. P. Gilbert, L. H. Teh, and H. Guan, "Self-shape optimisation principles: Optimisation of section capacity for thin-walled profiles," *Thin-Walled Structures*, vol. 60, pp. 194-204, 2012.

[12] B. W. Schafer and S. Adany, "Buckling analysis of cold-formed steel members using CUFSM: conventional and constrained finite strip methods," in *Eighteenth international specialty conference on cold-formed steel structures*, 2006: Citeseer, pp. 39-54.

[13] B. Wang, B. P. Gilbert, H. Guan, and L. H. Teh, "Shape optimisation of manufacturable and usable cold-formed steel singly-symmetric and open columns," *Thin-Walled Structures*, vol. 109, pp. 271-284, 2016.

[14] Rondo Buliding Service Pty Ltd*, Rondo STEEL STUD Framing Systems Installation Manual. 2008.*

[15] BlueScope Steel Limited*, LYSAGHT Zeds and Cees Users Guide. 2017..*

[16] *AS/NZS 4600: Cold-formed steel structures*, Standards Australia, 2005.

[17] B. W. Schafer and T. Pekoz, "Direct strength prediction of cold-formed steel members using numerical elastic buckling solutions," 1998.